

ARTICLE

Behavior of lap splices in reinforced concrete beams after bar yielding

Jukka Haavisto  | Heikki Alho | Anssi Laaksonen 

Faculty of Built Environment—Concrete and Bridge Structures, Tampere University, Tampere, Finland

Correspondence

Jukka Haavisto, Faculty of Built Environment—Concrete and Bridge Structures, Tampere University, P.O. Box 600, FI-33014, Tampere, Finland.
Email: jukka.haavisto@tuni.fi

Funding information

Finnish Concrete Industry

Abstract

Structural ductility in the case of plastic hinges forming close to a lap splice has been an open issue with the revision process of the next version of Eurocode EC2 concerning reinforced-concrete structures. This research has provided experimental evidence by the large experimental campaign for the background for revision of the Eurocode EC2. Within this context, 38 specimens were tested in four-point bending, with the longitudinal bars either lap-spliced (partly or fully), or un-spliced (for reference). The tests were carried out involving the variation of the bar diameter (12, 16, 20, and 25 mm), and the lap length (20–60 times the bar diameter). The main result is the sizeable enhancement of the structural ductility brought in by the extension of the lap length in excess of the length required by the yielding of the longitudinal bars. Based on these findings, a preliminary model is developed to describe the bond-stress profiles in lap splices, after the yielding of the bars.

1 | INTRODUCTION

Transportation and handling limitations have an effect on the maximum length of the reinforcing bars and very often the bars must be spliced in the structure on site. Stresses are usually transmitted from one bar to another by one of these three following methods: lap splices, welded splices, and mechanical couplers, with lap, splices being the most commonly used.

The lap must be long enough to transfer the acting steel stresses from one bar to another. In the case of tension bars, the failure usually occurs as a splitting failure but also as a pull-out failure which is both brittle in

nature.¹ If a lap splice is placed near a critical cross-section where the bending moment reaches the yielding moment, lap splices are requested not only to transfer the force corresponding to bars yielding but also to provide a sufficient deformation capacity.

Several parameters have an influence on the lap strength, which makes the design of the lap quite complex. Lap strength models are, therefore, mainly based on the experimental databases, as are the models published by Orangun et al.,² Canbay and Frosch,³ Esfahani and Kianoush,⁴ Cairns,⁵ and Schoening.⁶

The diameter and geometry of the bars, lap length, compressive strength of concrete, and confinement effect of both concrete and transverse reinforcement have a significant effect on the lap strength. Hence, the effect of individual parameters on lap strength has been studied experimentally by several researchers. A wide experimental program has been carried out, particularly by Chinn

Discussion on this paper must be submitted within two months of the print publication. The discussion will then be published in print, along with the authors' closure, if any, approximately nine months after the print publication.

This is an open access article under the terms of the [Creative Commons Attribution](https://creativecommons.org/licenses/by/4.0/) License, which permits use, distribution and reproduction in any medium, provided the original work is properly cited.

© 2023 The Authors. *Structural Concrete* published by John Wiley & Sons Ltd on behalf of International Federation for Structural Concrete.

et al.,⁷ Ferguson and Breen,⁸ Tepfers,⁹ Rezansoff et al.,¹⁰ Azizinamini et al.,¹¹ and Zuo and Darwin.¹² In each of the previous studies more than 30 lap splices were tested.

These and the test results of 25 other studies were included in the extended database prepared by *fib* Task Group 4.5¹³ which contains the results of over 800 tests. Based on this database, a semi-empirical equation for laps and anchorages presented in Model Code 2010¹⁴ and in *fib* Bulletin 72 was developed. This model and the changes in relation to the previous Model Code 1990¹⁵ were first published by Cairns.⁵

Major changes to the lap splice design are under process in the next version of Eurocode EC2¹⁶ compared to the current Eurocode EN1992-1-1:2004¹⁷ New design rules are going to be based on the *fib* Bulletin 72 semi-empirical model, which is slightly simplified and modified to be suitable for design purposes. Most of the studies in the background database are focused on lap lengths shorter than the yielding of the bars would require and this has raised concerns about the adequate ductility if the plastic hinge forms near the lap splice.

Although most experimental studies on lap splices have been focused on the lap strength in the elastic region, several test projects have been devoted also to long lap splices, where the yield strength of the lapped bars has been achieved. Darwin et al.,¹⁸ and Darwin¹⁹ examined an extended database including many test results and concluded that the yielding of the lapped bar does not have a significant effect on the lap strength unless the lapped bars are confined by transverse reinforcement which gives some benefit.

In most papers on the ductility of lap splices, the effect of one or more parameters is investigated, as in Mousa²⁰ study. Confining reinforcement is found to have an important role in the ductility of the lap-spliced beams²¹ and ductility can be improved by increasing the number of stirrups at the lap splice.^{22,23} Mabrouk and Mounir²⁴ found that a uniform distribution of the transverse reinforcement along the lap length is important for ductility. Gilbert and Kilpatrick²⁵ found that high ductility in lap splices can be more easily achieved when normal-strength concrete is used in RC beams, rather than high-strength concrete.

In most of the studies, the deflection-based ductility index^{23,26,27} or displacement ductility ratio^{11,20,21} have been used as an indicator of ductility, but the behavior of the lap splice in the plastic region has not been studied in depth. Micallef and Vollum²⁸ and Gillani et al.,²⁶ studied the local behavior of lapped bars after yielding by using the strain gauges in lapped bars. Haefliger et al.,²⁹ developed a mechanically consistent method for lap splices based on the tension chord model (TCM).^{30,31}

The aim of this study is to investigate the behavior of lap splices after yielding of the reinforcing bar. To this

aim, a total of 38 bending tests were performed on RC beams, in which the lap length was varied from 20 to 60 times the bar diameter. Such parameters or features like the lap capacity, the profile of the bond stresses along the lap length, and the maximum strain in the bars are investigated for various bar diameters and proportions of the lapped bars. In the case of long lap splices, the formation and rotation capacity of the plastic hinges are examined as well.

2 | EXPERIMENTAL PROGRAM

2.1 | Description of tests

A total of 38 test beams in four test series were loaded in four-point bending by varying the diameter of the bars ($\phi = 12, 16, 20,$ and 25 mm), the lap length (60, 50, 40, 30, and 20 times the longitudinal bar diameter) and the proportion of the lapped bars (100%, 50%, and 0%).

According to the *fib* Bulletin 72 semi-empirical model, the minimum lap length required by the yielding of the longitudinal bars was evaluated to be $27\phi, 28\phi, 32\phi,$ and 39ϕ for the specimens reinforced with 12, 16, 20, and 25 mm bars, respectively. Based on this, the maximum lap length was chosen to be 50ϕ at the beginning of the test program. However, after the results of the first series were analyzed, the lap length required by the yielding of the bars was found to be greater than the predefined value, and thus the lap length of 60ϕ is included in the last series of tests (100% lapped $\phi = 12$ mm and $\phi = 20$ mm specimens).

The bars on the tension side are lapped at the mid-span. There is a pure bending moment acting at the lap zone, except for the minor effects due to the own weight of the beams. The bars at the lap splice are arranged with the transverse ribs pointing to the smallest concrete cover.

The beams have a square cross-section with four longitudinal bars at the tension side. The beam dimensions are scaled to the bar diameter, as shown in Table 1. However, all beams have a constant 20 mm concrete cover on the stirrups which corresponds to the practical case where the thickness of the concrete cover is small. The concrete cover on the lapped bars is then 28, 30, 32, and 32 mm for 12, 16, 20, and 25 mm bars, respectively. The neutral axis-depth ratio of test specimens is quite low ($x_u/d = 0.13$ – 0.14). In that range, both concrete crushing and rupture of bar could occur nearly simultaneously. Hence, a high curvature of the beam is expected.

The size of the beam is chosen so that the distance of the internal lapped bars to the vertical leg of the stirrup is about 6ϕ . Confinement reinforcement is arranged with

TABLE 1 Geometrical details of the specimens and the dimensions of the test arrangement

	100% lapped				50% lapped				0% lapped			
ϕ (mm)	12	16	20	25	12	16	20	25	12	16	20	25
a_1 (mm)	20	20	30	30	20	20	30	30	20	20	30	30
a_2 (mm)	726.0	935.8	125 6.3	155 6.2	726.0	915.7	125 6.3	155 6.2	74	98	132	164
c_x (mm)	48	50	62	62	100	121	157	187	-	-	-	-
c_y (mm)	28 2.3	30 1.9	32 1.6	32 1.3	28 2.3	30 1.9	32 1.6	32 1.3	-	-	-	-
b (mm)	270	350	450	550	270	350	450	550	270	350	450	550
h (mm)	270	350	450	550	270	350	450	550	270	350	450	550
d (mm)	235	310	405	505	235	310	405	505	235	310	405	505
d_{sw} (mm)	8	10	12	12	8	10	12	12	8	10	12	12
Concrete batch no.	4	1	4	1	3	2	3	2	3	2	3	2
L_0 (m)	3.75 16.0	4.95 16.0	5.90 14.6	6.80 13.5	3.75 16.0	4.95 16.0	5.90 14.6	6.80 13.5	3.75 16.0	4.95 16.0	5.90 14.6	6.80 13.5
a_c (m)	1.25 5.3	1.65 5.3	2.10 5.2	2.60 5.1	1.25 5.3	1.65 5.3	2.10 5.2	2.60 5.1	1.25 5.3	1.65 5.3	2.10 5.2	2.60 5.1
a_v (m)	1.25 5.3	1.65 5.3	1.90 4.7	2.10 4.2	1.25 5.3	1.65 5.3	1.90 4.7	2.10 4.2	1.25 5.3	1.65 5.3	1.90 4.7	2.10 4.2

Note: d = effective depth; d_{sw} = stirrup diameter; L_0 = Span length; a_c = load span; a_v = shear span (see also Figure 4).

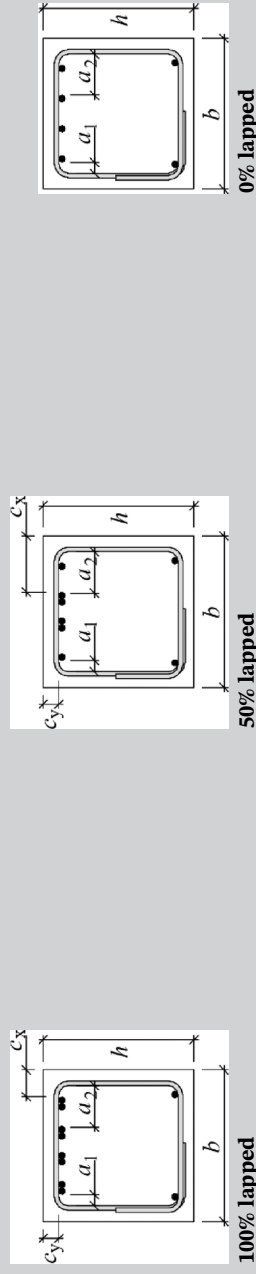




FIGURE 1 Casting of the test beams

constant spacing along the beam, which is considered to correspond best with the practical cases. The distance of the first stirrup from the lap end is, however, limited to a maximum of 50 mm. As a result of this, the spacing of the confinement reinforcement over the lap length is in some specimens slightly wider than in other specimens. This is noticeable also in the differences in densities of confining reinforcement (so-called K_{tr} values) in Table 4. The density of confining reinforcement is quite low in all the tested lap splices.

2.2 | Materials and casting

All test series were cast with similar concrete supplied by a local ready-mix company. The target compressive strength of the concrete was $f_c = 35$ MPa with a maximum aggregate size of 16 mm. The concrete was produced with CEM I SR3 52,5N cement. Concrete was transferred by pumping (Figure 1) and was primarily highly workable (measured slump according to EN 12350-2³² varied between 190 and 250 mm).

The concrete compressive strength was determined for each batch by conducting tests on water-soaked 150×300 cylinders at the age of 28 days ($f_{cm,28}$) and on 150×300 cylinders under the same storage conditions and at the same testing age as the RC beams ($f_{cm,test}$). The splitting tensile strength was tested for each batch on 150×300 cylinders stored on similar conditions and tested at a similar age as the RC beams ($f_{ctsm,test}$). Compressive tests were carried out in accordance with EN 12390-3³³ while the splitting tensile tests were obtained in accordance with EN12390-6.³⁴ The average values are reported in Table 2.

As the properties of the bars have a significant effect on their bond behavior, tensile tests and geometrical analyses

in accordance with EN ISO 15630-1³⁵ were conducted on steel samples in a certified laboratory for each batch of hot-rolled reinforcing bars used in test beams. The parameters of the bars are summarized in Table 3. The material yield strength varied from 521 to 588 MPa which is a typical value for B500 strength class structural steel. The relative rib area was $f_R = 0.076$ – 0.094 which is 1.4–2.4 times greater as required by Eurocode 2 (2015) for sufficient bond properties ($f_{R,min} = 0.040$ and $f_{R,min} = 0.056$ for 12 mm and 16–25 mm bars, respectively). As shown in the studies by Cairns and Jones³⁶ and Metelli and Plizzari³⁷ such a relative rib area may improve the bond strength of the specimens by a maximum of 30%, compared to the bars whose relative rib area is equal to the Eurocode minimum requirements.

It is noteworthy here that bars with $\phi = 12$ -mm-diameter were straightened from a coil and, therefore, the stress–strain relationship is different than in other studied bar sizes (Figure 2) as there is no yield plateau in the behavior of straightened bars.

The test specimens were cast with the lapped bars placed at the bottom side of the mold. The good bond conditions can be, thus, assumed.^{14,16,38} The beam specimens were covered with a plastic film for 14 days and then were demoulded. Subsequently, the specimens were rotated by 180° in order to have the lapped bars in the top position during the tests.

2.3 | Test setup

The bending tests were carried out on beam-like specimens with the tension side upwards, as shown in Figure 3. This loading direction helps to make better observations in the lap region and has also been used in several other studies (Azizinamini et al.,⁸ Ferguson and Breen,³⁹ Schoening and Hegger⁴⁰). The tests were conducted with the load span ratio (a_0/d) of around five and span length ratio (L_0/d) from 13.5 to 16.0 depending on the specimen size (see details in Table 1). As the specimens were loaded upside-down with the tension side at the top, the span length L_0 is the total distance between the two load points (at the extremities), while the load span a_0 (subjected to pure bending) is the distance between the two-fixed supports and the shear span a_1 is the distance between each fixed support and the nearest extremity. In the specimens reinforced with 12 mm and 16 mm bars, the shear span is equal to the load span ($a_1 = a_0 = 1/3 \cdot L_0$), while in the specimens reinforced with 20 mm and 25 mm bars the shear span is reduced ($\phi = 20$ mm: $a_1 \approx 0.9a_0$ and $\phi = 25$ mm: $a_1 \approx 0.8a_0$) because of some limitations in the stroke of the pistons of the actuators.

The servo-hydraulic cylinders with ball joints at both ends were displacement-controlled with an initial rate of

TABLE 2 Concrete strength results

Batch	$f_{cm;28}$ (MPa) $n = 3$	$f_{cm;test}$ (MPa) $n = 6$	$f_{ctsm;test}$ (MPa) $n = 6$
1	32.4	36.4	2.8
2	33.0	41.0	3.2
3	28.4	31.0	2.7
4	30.9	34.4	2.8

TABLE 3 Steel properties

ϕ (mm)	R_{eH} (MPa)	R_m (MPa)	A_{gt} (%)	f_R	c (mm)	b_r (mm)	α ($^\circ$)	β ($^\circ$)	Test beams
12	529 ($R_{p0.2}$)	634	9.5	0.094	7.0	2.0	48	52	All B12-beams
16	565	664	10.0	0.076	9.7	1.9	48	54	B16-20-100
16	521	615	11.5	0.078	10.0	1.6	50	53	Rest of the B16 -beams
20	540	621	11.0	0.090	10.7	2.1	49	59	All B20 -beams
25	526	616	11.0	0.090	12.4	2.4	49	60	B25-50-100
25	558	656	10.0	0.080	12.7	2.9	49	59	B25-40-100
25	560	655	10.0	0.082	12.7	2.8	48	59	B25-30-100
25	562	657	10.0	0.082	12.7	2.7	49	59	B25-20-100
25	573	659	10.5	0.078	12.8	2.5	56	60	B25-REF
25	588	700	9.0	0.077	12.8	2.2	51	60	All 50% lapped B25 -beams

Note: c = transverse rib spacing (average value); b_r = width of transverse rib measured parallel to the axis of the bar; α = transverse rib flank inclination; β = angle between the axis of a transverse rib and the bar (average value).

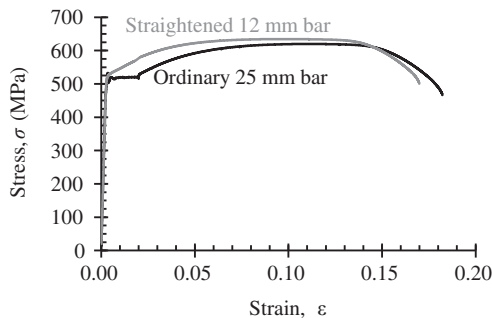


FIGURE 2 Stress-strain curves of a straightened bar ($\phi = 12$ mm, thin curve) and of an ordinary bar ($\phi = 25$ mm, thick curve)

1.0 mm/min until the reinforcement yielded. Thereafter, the displacement rate was increased.

The applied load was measured by the load cells of the actuators. Strain gauges were mounted along the lap length, as shown in Figure 4. Strain gauges were also installed on the same bars at the supports. The rotation of the beam was measured at the supports with the measuring rod with two horizontal displacement transducers at each. Deflection of the beam was measured at both loading points and at the mid-span. In addition, the digital image correlation (DIC)

technique was used to determine the deformations on the one side surface of the beam. The longitudinal strain was also measured with displacement transducers at the top and bottom surfaces of the beam, but the results of these measurements are not used in the analysis.

3 | RESULTS AND DISCUSSION

3.1 | Lap strength

Since the concrete net cover was limited to 3 bar diameters, a splitting-type failure was expected in all cases (Cairns,⁵ *fib* Bulletin 72). In fact, all specimens failed because of splitting, as clearly indicated by the crack patterns during the tests and by the post-failure behavior.

The ultimate deflection of the reference beams (with continuous bars) was greater than that of the corresponding lap-spliced beams, and, thus, the reference beams exhibited a more ductile behavior. The reference beam with $\phi = 12$ mm reinforcement (B12-REF) failed due to a rupture of the bars on the tension side. In other reference beams, the loading process was continued until the maximum piston stroke of the hydraulic jack was achieved. At that time, a severe spalling of concrete was observed on

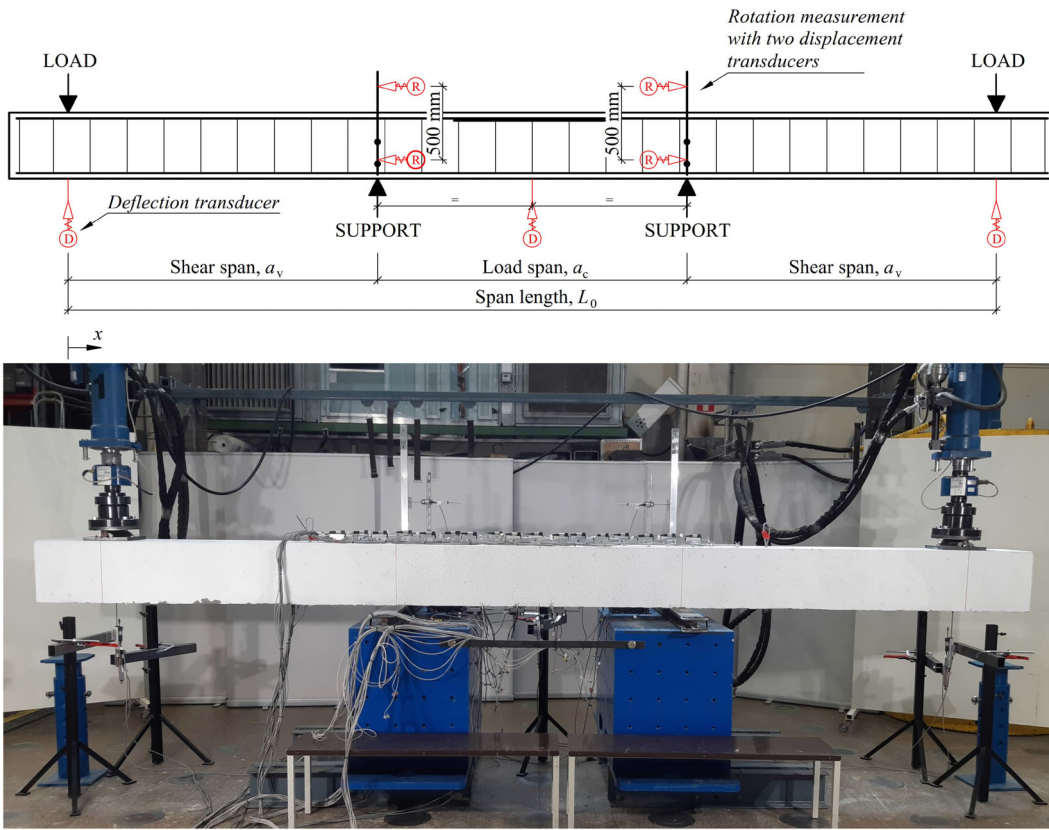


FIGURE 3 Test setup

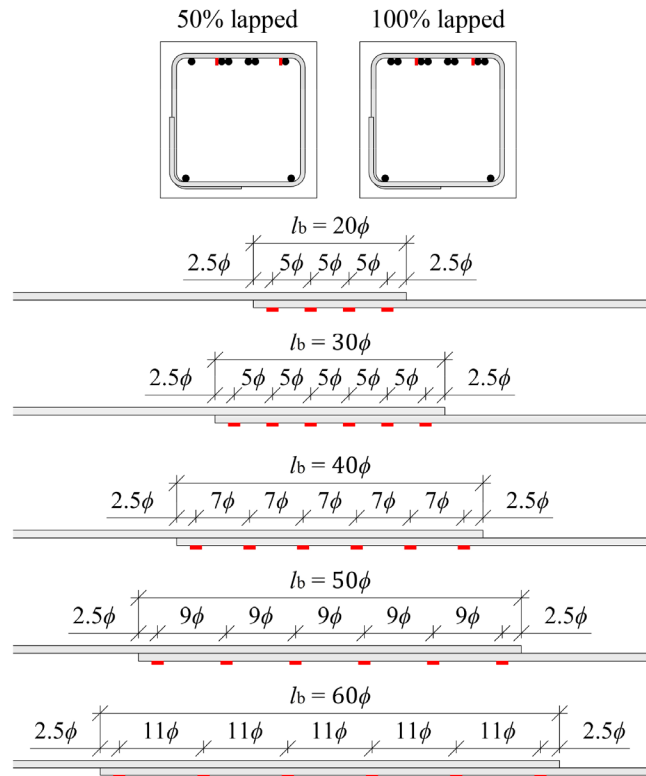


FIGURE 4 Strain gauge positions

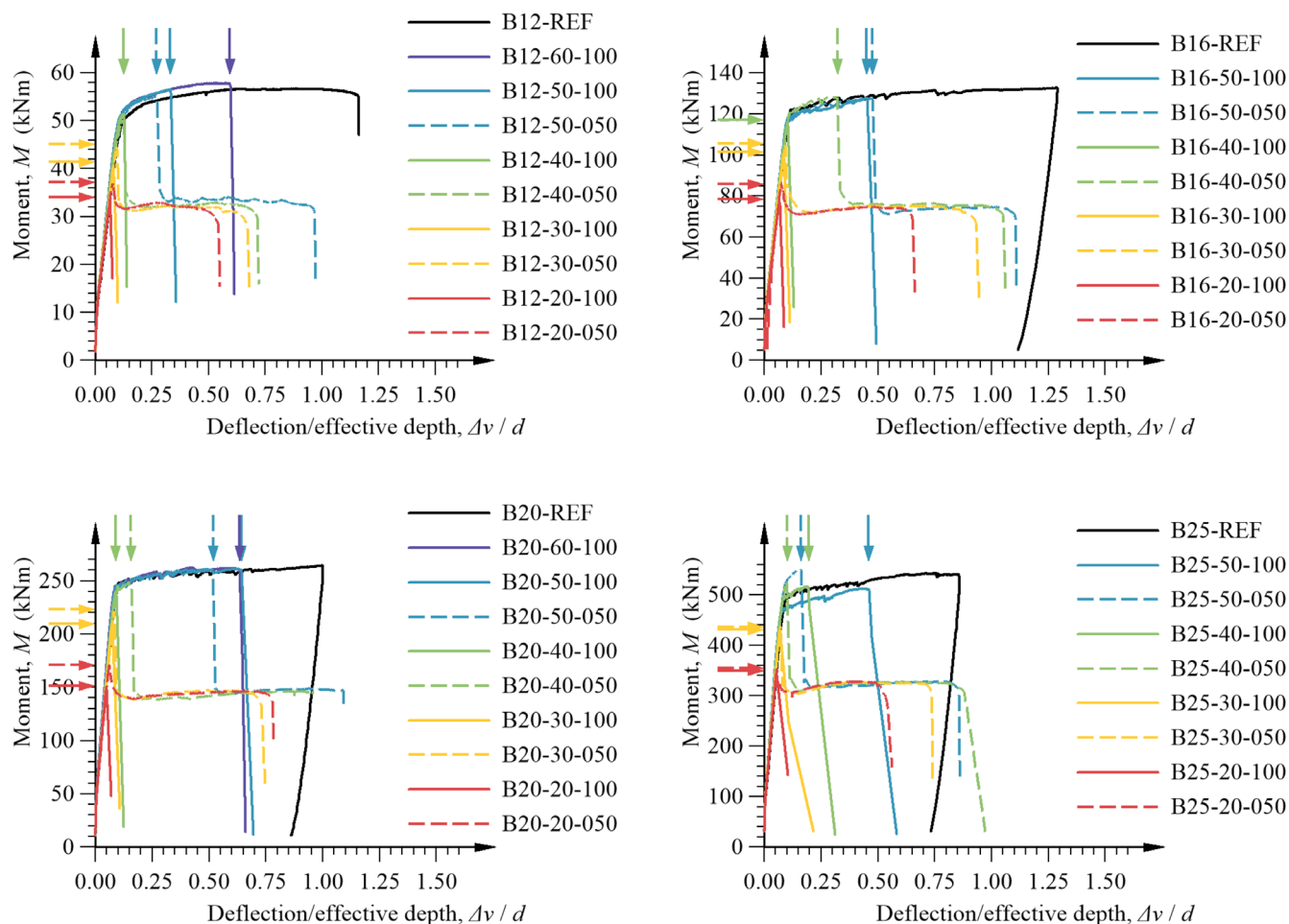


FIGURE 5 Moment-deflection curves of test specimens

the compression side of all these specimens, although no significant drops in the applied load were observed.

The strength and ductility behavior of RC beams with different lap lengths can be easily observed from the moment-deflection curves in Figure 5, which use the ratio of deflection to effective depth to facilitate a comparison between different sizes of beams. Deflection values Δv are expressed here as the average difference in vertical displacement between the loading points ($x = 0$ and $x = L_0$ according to Figure 3) and the mid-span ($x = 0.5 \cdot L_0$).

The short lap splices failed before the yielding of the tension bars. Based on the results, a lap length close to 40 bar diameters (40ϕ) appears to be sufficient to transfer a tensile force equal to the yield load of B500 bars in these test series.

The measured lap strengths of short lap splices were compared to those resulting from code equations in a previously published paper.⁴¹ The lap strength was found to follow the model of *fib* Bulletin 72, the provisions of current Eurocode (EN 1992-1-1:2015),¹⁷ and the draft of second-generation Eurocode¹⁶ with good precision if no confinement effect was taken into account.

The effectiveness of the confinement against the splitting failure has been found to be dependent on the distance of the anchored bar to the nearest vertical link in several studies as the confinement is more effective against the side cracks than the face cracks.^{42–44} In this study, the distance of the middle lap joint to the confinement reinforcement was about 6ϕ in all lap-spliced specimens. This is greater than the limit value of 5ϕ , which would allow us to take into account the full positive effect of the confinement reinforcement in a lap splice design according to *fib* Bulletin 72 and to the draft of second-generation Eurocode.¹⁶ However, since the distance is less than 125 mm in specimens reinforced with small- and medium-diameter bars ($\phi = 12, 16,$ and 20 mm), the favorable effect of the nearest vertical link could be taken into account according to *fib* Bulletin 72. Based on the test results of this study, this limit of 125 mm is questionable, and it seems to be an appropriate option to exclude it from the draft of second-generation Eurocode.¹⁶

The effect of the distance limit value of 5ϕ is radical in the model of *fib* Bulletin 72. When the limit is exceeded, the calculated effect of the confinement of the

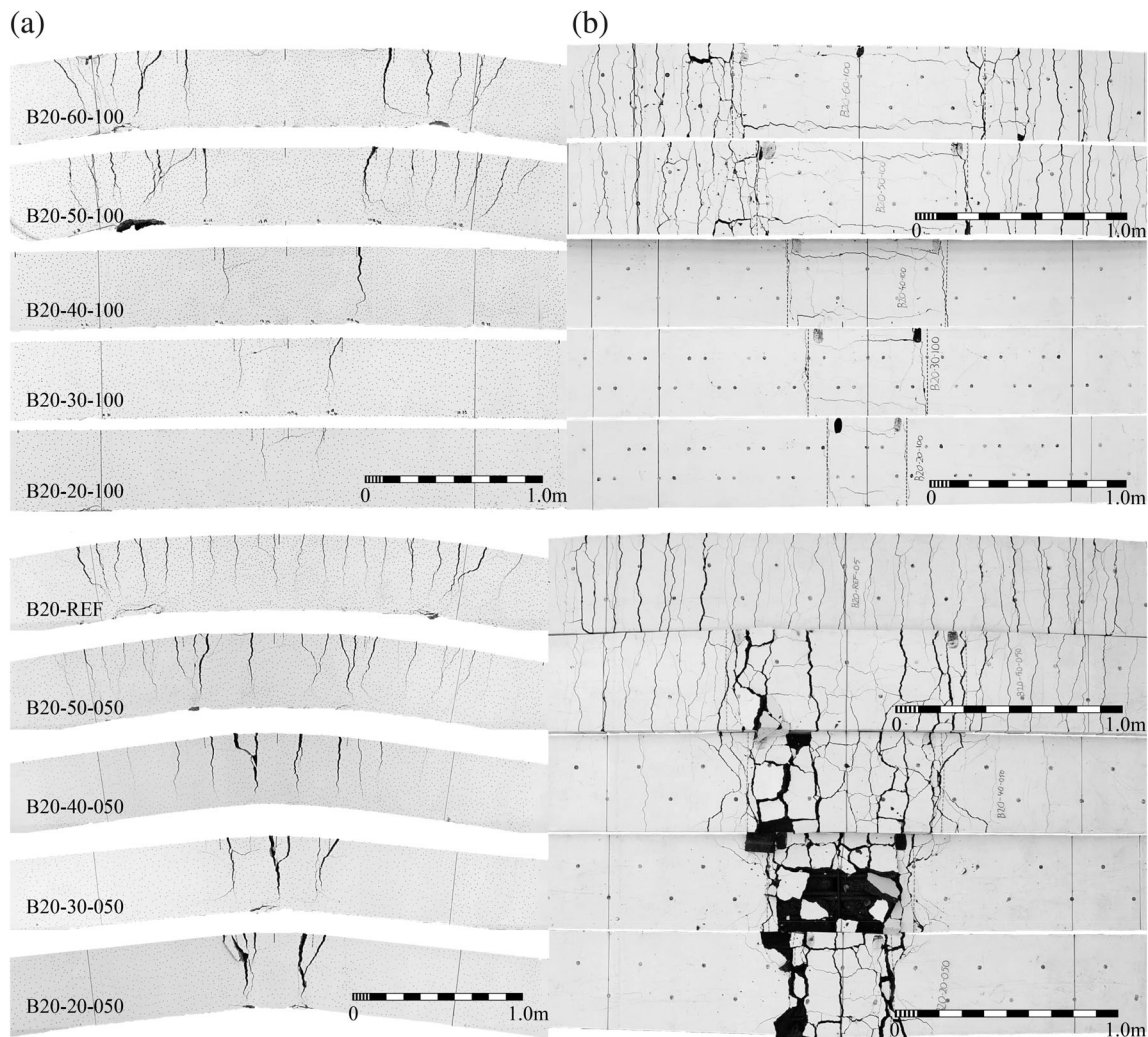


FIGURE 6 Crack patterns after failure for $\phi = 20$ mm test specimens (a) side view; (b) top view (tension side). The lap ends, the mid-span, and the support lines of the beams are marked with the vertical lines.

confinement reinforcement to the lap strength changes from full to zero if the clear spacing between the laps is low, as in these test specimens. The authors suggest that the change in the calculated effect of the confinement should be not so sharp, and instead it should change more smoothly.

In longer lap splices, the failure occurred after the yield strength of the bars was achieved and, thus, there are only minor differences in their moment capacities. The measured deflection at the failure is also quite similar among the beams with equal lap length but different shares of the lapped bars. In several cases, a deflection at the maximum moment is even higher in 100% lapped specimens than in similar beams with only 50% of bars lapped. The proportion of the lapped bars has no significant effect on lap strength, neither in short lap splices, albeit in all these cases the ultimate value is slightly higher in beams with 50% of bars lapped than in beams with 100% of bars lapped.

These observations raise questions about the need for staggering the lap splices and about the need for *increasing* the lap length in terms of lap strength if all bars are *lapped* at one cross-section. This has been required in many design codes such as in ACI 318-19⁴⁵ and EN 1992-1-1:2015.¹⁷ Cairns⁴⁶ and Metelli et al.,⁴³ came to a similar conclusion about the need for staggering the laps in their experimental studies. However, the crack width at the serviceability limit state is not analyzed in this research project, even if crack width may benefit from the staggering of the laps.

For specimens reinforced with medium- and large-diameter bars ($\phi = 16, 20,$ and 25 mm) the yield point can be easily identified from the sharp slope discontinuity in the moment-deflection curves. However, in the test series of RC beams reinforced with 12 mm bars straightened from the coil, the moment-deflection response is rounded, and a sharp yield point cannot be identified. In this regard, it can be stated that the use of straightened

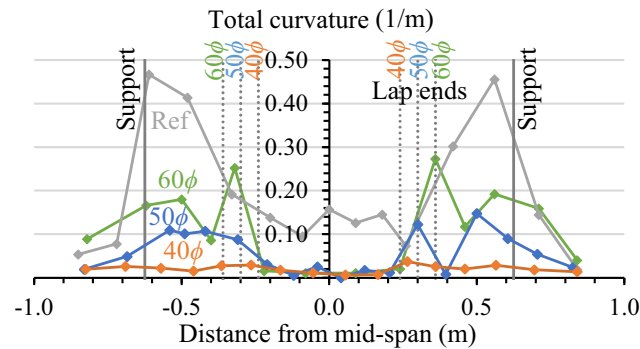


FIGURE 7 Total curvature (elastic + plastic) distribution for 100% lapped 40–60 ϕ test specimens with $\phi = 12$ mm bars and a corresponding reference beam. Loading points are located at a 1.875 m distance from the mid-span.

bars in reinforced concrete beams has some effect on their plastic behavior.

A sudden drop of the applied load was observed after the failure in all lap-spliced specimens. The beams with all the bars lapped in a single section provided no significant residual strength after splitting of the concrete cover, while the beams with 50% of bars lapped provided the residual strength of more than half of the cross-section moment capacity, which is in agreement with the findings of Maurer and Bettin.⁴⁷ In the residual stage of the beams with 50% of bars lapped the cross-section had a very low amount of reinforcement when only two active bars at the tension side were left. That was also noticeable at the very end of the loading process when, in some specimens, the high-strain deformations resulted in the necking of the bars.

3.2 | Crack patterns

Figure 6 shows the final crack patterns for the test specimens reinforced with $\phi = 20$ mm bars at an unloaded state after tests. Crack developments in other series were qualitatively the same. The plastic deformations stand out particularly well in the unloaded state, as the cracks in the elastic region are mainly closed.

The crack pattern in Figure 6 is clearly different between the beams with 50% of bars lapped and the beams with respective lap lengths but 100% of bars lapped, as in the former case the cracks are wider and there are also flexural cracks within the lap region. However, until the maximum bending moment was reached, the crack patterns were more similar, as the flexural cracks in the lap-spliced zone appeared mainly during the post-peak loading. Only a few individual new cracks appeared in test specimens during the strain hardening stage.

In the case of the reference beam, the major cracks are distributed over the whole constant moment area.

The plastic region is, therefore, fairly extended, which results in a high ductility of the beam. Instead, in beams with 100% of bars lapped, two plastic hinges can be noticed, one on both lap ends. The cracks outside the constant moment area are slightly diagonal due to the shear stresses.

Longitudinal splitting cracks in lap-spliced beams are wider at the top surface (tension side) than at the side surfaces, probably because c_x is in all beams much thicker than c_y .

3.3 | Plastic rotation

All lapped specimens with the lap length of 50 ϕ and 60 ϕ were able to form a plastic hinge before failure. In specimens with 40 ϕ lap length, the failure occurred very close to the yield point of the reinforcement, and thus in some of these, the yielding of the bars was observed, while in others the failure occurred during the elastic phase.

Bar plasticization occurred mainly in the constant-moment region between the supports, but outside the lap-spliced zone. However, some plasticization was observed also in the sections between each support and the nearest extremity, as can be seen in Figures 6–8.

Figure 8 shows the distribution of the plastic curvature along the beam for the 50 ϕ lapped specimens in both used proportions of the lapped bars and for the reference beam for $\phi = 20$ mm test series. The distribution is determined here by using DIC technology. Due to the sparse speckle pattern, the number of the observation points between the different test beams differ markedly from each other. Therefore, the graph shows the average curvature for each measuring distance, which makes the results more comparable. Figure 7 shows the distribution of the maximum curvature for a 100% lapped $\phi = 12$ mm test series with long lap splices.

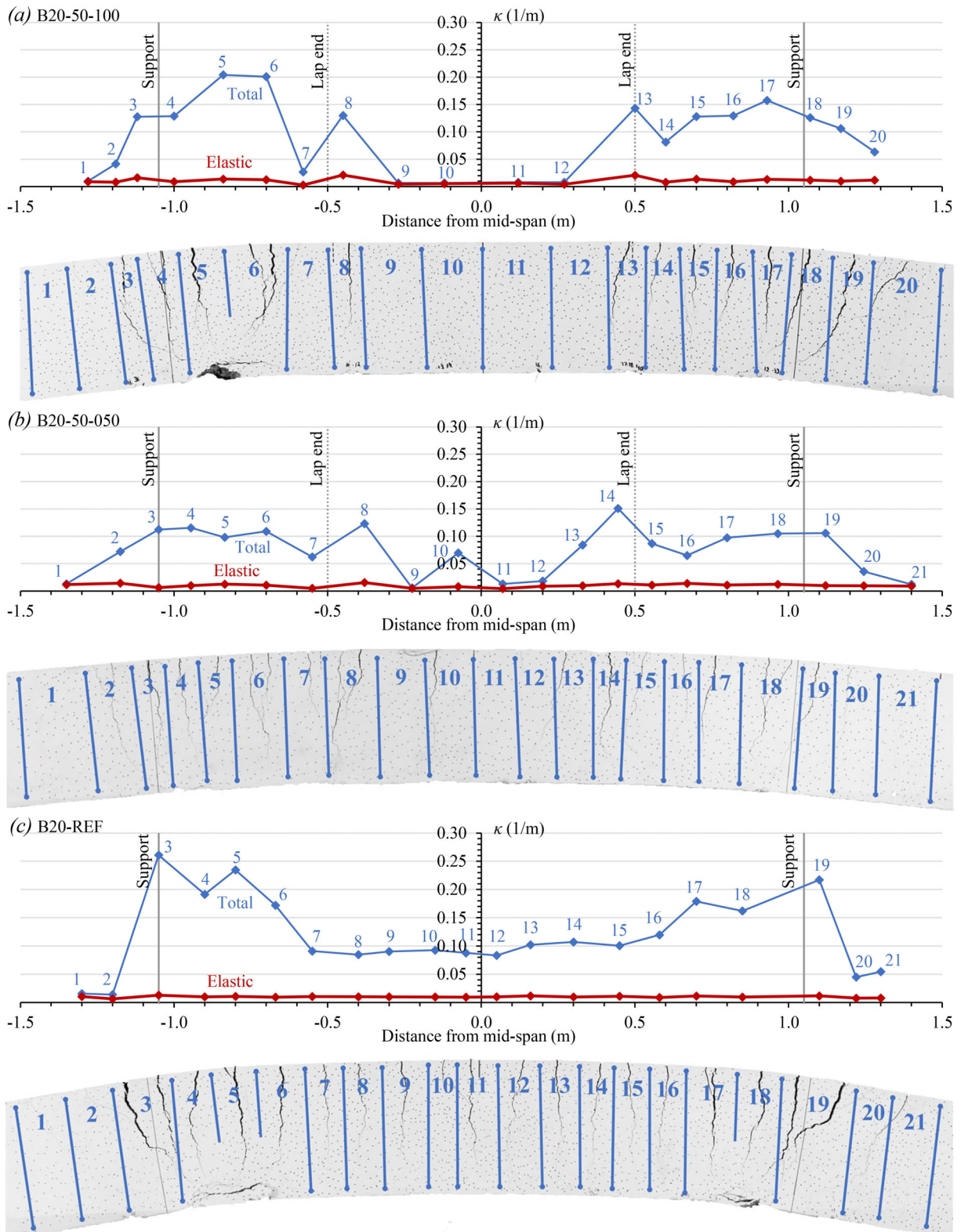


FIGURE 8 Curvature distribution for (a) test specimen B20-50-100; (b) test specimen B20-50-050; and (c) test specimen B20-REF. Loading points are located at a 2.95 m distance from the mid-span.

TABLE 4 Test results and transverse reinforcement parameters

ϕ (mm)	Test specimen	l_b/ϕ	n_b	n_g	K_{tr}	M_{max} (kNm)	σ_{su} (MPa)	ϵ_{sm}	$\epsilon_{s,max}$ (‰)
12	B12-60-100	60	4	5	0.015	57.9	$> f_y$	0.036	0.057
	B12-50-100	50	4	4	0.014	56.6	$> f_y$	0.021	0.043
	B12-40-100	40	4	3	0.013	51.4	529	$< \epsilon_{sy}$	$< \epsilon_{sy}$
	B12-30-100	30	4	2	0.012	40.7	426	$< \epsilon_{sy}$	$< \epsilon_{sy}$
	B12-20-100	20	4	2	0.017	33.4	352	$< \epsilon_{sy}$	$< \epsilon_{sy}$
	B12-50-050	50	2	4	0.028	55.0	$> f_y$	0.015	0.041
	B12-40-050	40	2	3	0.026	50.1	$> f_y$	0.004	0.011
	B12-30-050	30	2	2	0.023	44.5	469	$< \epsilon_{sy}$	$< \epsilon_{sy}$
	B12-20-050	20	2	2	0.035	36.8	394	$< \epsilon_{sy}$	$< \epsilon_{sy}$
B12-REF	–	0	–	–	56.8	$> f_y$	0.032 ^a 0.084 ^b	0.048 ^a	
16	B16-50-100	50	4	4	0.012	127.6	$> f_y$	0.033	0.063
	B16-40-100	40	4	4	0.015	116.4	519	$< \epsilon_{sy}$	$< \epsilon_{sy}$
	B16-30-100	30	4	3	0.015	100.9	452	$< \epsilon_{sy}$	$< \epsilon_{sy}$
	B16-20-100	20	4	2	0.015	77.8	346	$< \epsilon_{sy}$	$< \epsilon_{sy}$
	B16-50-050	50	2	4	0.025	127.4	$> f_y$	0.030	0.042
	B16-40-050	40	2	4	0.031	128.0	$> f_y$	0.016	0.031
	B16-30-050	30	2	3	0.031	104.5	463	$< \epsilon_{sy}$	$< \epsilon_{sy}$
	B16-20-050	20	2	2	0.031	85.8	386	$< \epsilon_{sy}$	$< \epsilon_{sy}$
	B16-REF	–	0	–	–	132.6	$> f_y$	0.043 ^a 0.072 ^b	0.070 ^a 0.100 ^b
20	B20-60-100	60	4	5	0.012	262.2	$> f_y$	0.051	0.090
	B20-50-100	50	4	4	0.011	261.3	$> f_y$	0.036	0.067
	B20-40-100	40	4	4	0.014	240.0	521	$< \epsilon_{sy}$	$< \epsilon_{sy}$
	B20-30-100	30	4	3	0.014	208.3	454	$< \epsilon_{sy}$	$< \epsilon_{sy}$
	B20-20-100	20	4	2	0.014	151.0	329	$< \epsilon_{sy}$	$< \epsilon_{sy}$
	B20-50-050	50	2	4	0.023	260.9	$> f_y$	0.035	0.058
	B20-40-050	40	2	4	0.028	248.8	$> f_y$	0.009	0.038
	B20-30-050	30	2	3	0.028	220.9	483	$< \epsilon_{sy}$	$< \epsilon_{sy}$
	B20-20-050	20	2	2	0.028	171.1	375	$< \epsilon_{sy}$	$< \epsilon_{sy}$
	B20-REF	–	0	–	–	264.3	$> f_y$	0.035 ^a 0.063 ^b	0.058 ^a 0.089 ^b
25	B25-50-100	50	4	7	0.013	512.1	$> f_y$	0.044	0.065
	B25-40-100	40	4	5	0.011	516.5	$> f_y$	0.013	0.030
	B25-30-100	30	4	4	0.012	432.5	488	$< \epsilon_{sy}$	$< \epsilon_{sy}$
	B25-20-100	20	4	3	0.014	346.6	390	$< \epsilon_{sy}$	$< \epsilon_{sy}$
	B25-50-050	50	2	7	0.025	550.4	$> f_y$	0.006	0.013
	B25-40-050	40	2	5	0.023	523.2	586	$< \epsilon_{sy}$	$< \epsilon_{sy}$
	B25-30-050	30	2	4	0.024	438.2	491	$< \epsilon_{sy}$	$< \epsilon_{sy}$
	B25-20-050	20	2	3	0.027	352.8	397	$< \epsilon_{sy}$	$< \epsilon_{sy}$
	B25-REF	–	0	–	–	542.8	$> f_y$	0.037 ^a 0.051 ^b	0.046 ^a 0.060 ^b

^aSteel strain at the same location than analyzed in lap-spliced specimens (lap end).

^bSteel strain at the supports; n_b = the number of pairs of lapped bars; n_g = the number of groups of links within the lap; $K_{tr} = (n_l \cdot n_g \cdot A_{sv}) / (l_b \cdot \phi \cdot n_b)$; n_l = the number of legs of a link in each group which cross the potential splitting failure plane ($n_l = 2$ in all specimens); A_{sv} = the area of each leg of a link.

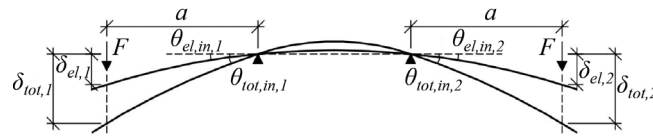


FIGURE 9 Defining the plastic rotation at outside of the supports from the test results

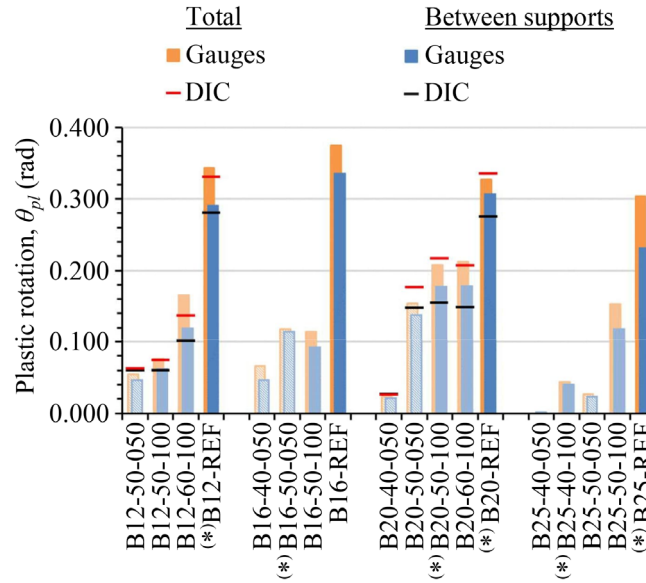


FIGURE 10 Plastic rotation levels of the yielded test beams

The results of the 100% lapped specimens confirm the previous observation of two separate plastic joints outside the lap-spliced region. The same trend can also be observed in 50% of lapped specimens, though some plastic deformations also occurred in the central region of the lap splices before the ultimate load.

Locally, the largest plastic rotation occurs at the lap ends, where bond is presumably rather weak due to the initial concrete splitting and the slip between the lapped bars reaches its largest value. The results also point to the high plastic rotation at the supports. This is especially pronounced in the reference beams, which did not even have a point of discontinuity in the reinforcement on the tension side caused by the lap splice. The high plastic rotation near the supports is probably formed due to the acting shear force on the beam outside the constant moment region, which have a beneficial effect on the plastic rotation due to the additional tensile force caused by shear-shifting. In addition, the bending moment caused by the self-weight of the beam is slightly higher at the supports than at the mid-span. This might have also some impact on the increased plastic deformations at the supports.

Plastic rotation at the constant moment region, $\theta_{pl,in}$, can be derived from the measurement results of the rotation

gauges at the support points of the beam with Equation 1. The plastic rotation that occurred outside the constant moment area, $\theta_{pl,out}$, can be calculated through the measured rotation results at the supports and the measured deflection results at the load points by using Equation 2

$$\theta_{pl,in} = \sum_{i=1}^2 (\theta_{tot,in,i} - \theta_{el,in,i}), \quad (1)$$

$$\theta_{pl,out} = \sum_{i=1}^2 \left(\frac{\delta_{tot,i} - \delta_{el,i}}{a} - (\theta_{tot,in,i} - \theta_{el,in,i}) \right), \quad (2)$$

where $\delta_{tot,i}$ is the vertical displacement measured at the loading point i before failure; $\delta_{el,i}$ is the vertical displacement measured at the loading point i at the yield point; $\theta_{tot,in,i}$ is the rotation measured at the support i before failure; $\theta_{el,i}$ is the rotation measured at the support i at the yield point; and a is the distance between the loading point and the support (Figure 9).

In all lapped specimens, the plastic rotation capacity is significantly lower than in the reference beams. Probably the most significant reason for this is the larger amount of reinforcement in the lap-spliced region, whereby the bending stiffness of the lap-spliced cross-

section is substantially higher when compared to the rest of the beam. In other words, when the bars at the tension side yield outside the lap splice, the bars at the lap-spliced region are still mainly in the elastic phase. For such a reason, the plastic region of the beam is much shorter in lapped specimens than in the corresponding reference beam. This is particularly evident in the $\phi = 20$ mm test series, where the concrete in the compression zone of the beam was crushed in 50ϕ and 60ϕ lapped specimens before the lap failure. This indicates the incipient bending failure of the cross-section, which was also observed in the corresponding reference beam. However, the total rotation in the reference beam is about 1.5 times the total rotation in these lap-spliced specimens (Figure 10).

Figure 10 shows the plastic rotation values of all the yielded specimens. All deformations that occurred since the yield point of the reinforcement was achieved are included in these plastic rotation values. The values are divided into the plastic rotation measured from the constant moment region (Equation 1) and the plastic rotation outside the supports, defined by Equation 2. In some of these test specimens, a bending crack crossed through the attachment point of rotation gauge at one support, and, therefore, the measured rotation was obtained only from the other support. In these specimens, the total rotation is estimated to be twice that of the measured value from the still-active gauge, see tags (*) in Figure 10.

In the tests where the bar diameter is equal to 12 and 20 mm, the total plastic rotation is evaluated also via DIC analysis and the agreement with the results provided by the gauges turned out to be more than satisfactory. Compared to the DIC results, in $\phi = 20$ mm test series the rotation gauge results are found to slightly underestimate the plastic rotation that occurred outside the supports. This is probably due to the diagonal cracks exceeding the support line above the attachment point of the rotation gauges. One difference in these measurements is also that in DIC analysis the whole span is not included. However, the deformations outside the measuring range appear to be smaller as they are still in the elastic region.

3.4 | Strain and stress distribution

The distribution of the bond stress along the lap splice is obtained from the strain gauge results for 100% lapped specimens. Steel stresses are determined based on the measured steel strains by using the *bilinear strain hardening model for the steel*. Based on the changes in steel stresses $\Delta\sigma_s$, the average bond stress for the distance between the strain gauges Δl is determined using the whole perimeter of the bar as follows:

$$\tau = \frac{\Delta\sigma_s \cdot \phi}{4 \cdot \Delta l}. \quad (3)$$

The measured steel strains and resulting bond stresses at different stages of the bending test for $\phi = 12$ mm and $\phi = 20$ mm 100% lapped specimens with a $40\text{--}60\phi$ lap length are shown in Figure 11. Since the measured strain is affected by tension stiffening, its values depend on the position of the strain gauges with respect to the cracks. However, the results give a fairly good overall view.

It can be seen from the results that at low steel stress levels, bond stresses occur only at the ends of the lap splice, and when the steel stress increase, the magnitude of the bond stress at the lap ends increases, and bond stresses occur in a larger area. For short lap splices, where the failure of the lap splice occurs before the yielding of the bars, the bond stress at the failure is almost constant over the entire lap length. This means that the steel stress increases almost linearly from one lap end to another up to the failure.

In long lap splices, where the yield strength of the bar was reached, the measured strains at the end of the lapped bar decrease after yield stress, which indicates a bond slip at the lap ends as a result of the high deformation of the bar. Meanwhile, the bond stress is increasing in the mid-section of the lap splice. As the deformation of the steel increase, the maximum bond stress shift from the lap ends toward the middle of the splice. The failure occurs when the maximum value is reached in the middle of the lap splice. The bond stress at the mid-splice is similar in all 100% lapped test specimens at the failure, roughly 1.5 times the splitting tensile strength of concrete. Figure 12 shows, schematically, the steps of the bond stress development for long and short lap splices, based on the results. The influence of bending cracking on bond stresses is neglected here.

The average steel strain at the failure, ϵ_{sm} , is determined in the DIC analysis over the widest cracks, i.e., over 2–3 cracks at both lap ends. Based on this, the steel strain at the crack, $\epsilon_{s,max}$, is evaluated by using the TCM.^{30,31}

For example, for test specimen, B20-50-100 ϵ_{sm} is evaluated from sectors 6–8 and 13–14 in Figure 8 (a). Both lap ends are analyzed individually but $\epsilon_{s,max}$ given in Table 4 is the average value from both lap ends. The strain values of other lapped specimens are determined in the same way.

In the reference beams, the average steel strain at the failure is evaluated at two different locations. Firstly, near the supports where the widest cracks in the beam are located. Secondly, in the location, which corresponds best to the analysis area used in lapped specimens. For example, for test specimen B20-REF, the average strain at the

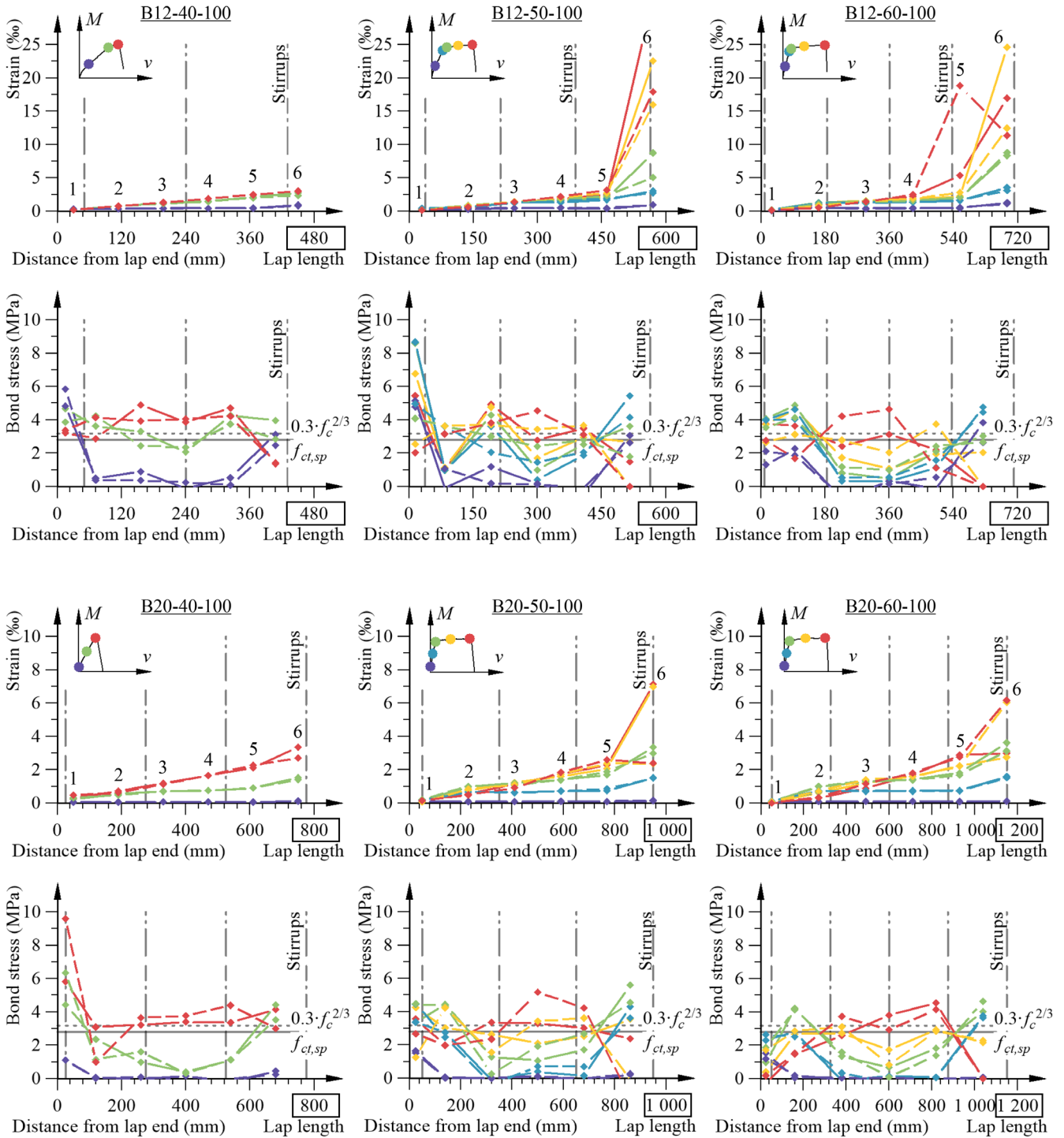
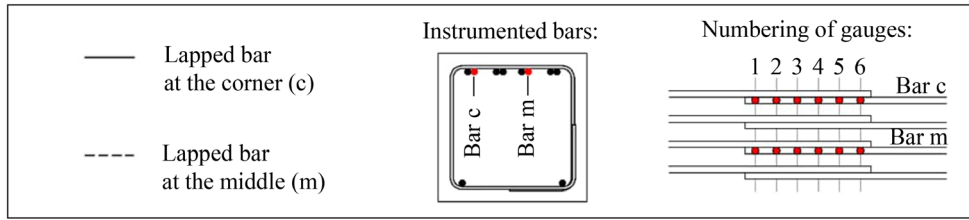


FIGURE 11 Strain and bond stress distribution for 100% lapped $\phi = 12$ mm and $\phi = 20$ mm specimens with 40–60 ϕ lap length

supports is evaluated from sectors 4–5 and 17–18 in Figure 8c. The other sectors analyzed in that specimen are 7–8 and 14–15 which correspond roughly to the analyzed locations in lap-spliced specimens. The steel strain evaluation among the reference beams is performed as similarly as possible. In some reference beams the DIC measuring range extended only up to the support lines and, therefore, cracks outside the support lines are not included in the analysis in any of the reference beams.

It is important to note that the evaluation of the maximum strain in this way is a bit dubious, as it is influenced—for instance—by crack formation. Such an evaluation, however, is performed to quantify the order of magnitude of the steel strain just before the lap-splice failure. The results concerning the maximum strain in the reinforcement in the specimens with lapped splices, which reached the yield strength of the bars before the

lap splice failed, show that higher deformations can be achieved by increasing the lap length (Figure 13a).

In lapped specimens with $\phi = 12$ mm reinforcement, the maximum steel strain at beam's failure can be observed to be lower than in other beams. This is probably due to the different stress–strain behavior of the bars straightened from the coil. Consequently, the bars do not exhibit a plastic plateau and strain hardening begins immediately after bar yielding. Test specimens with 12 mm bars also have the highest f_R value which leads to a lower crack spacing, and the highest c/ϕ ratio which might have an effect on the obtained test results because of a lower reinforcement ratio at the tension chord. The $\epsilon_{s,max}$ value in B25-50-050 specimen is affected by a clearly higher yield strength of reinforcement ($f_y = 588$ MPa) than other yielded test specimens ($f_y = 521$ – 558 MPa) in which case a longer lap splice is required to transfer the yield stress.

The crack spacing is one of the input data of the TCM. As the analysis here is made only over 2–3 cracks and crack spacing is characterized by a sizeable dispersion, Figure 13b shows also the $\pm 25\%$ error bars for the crack spacing.

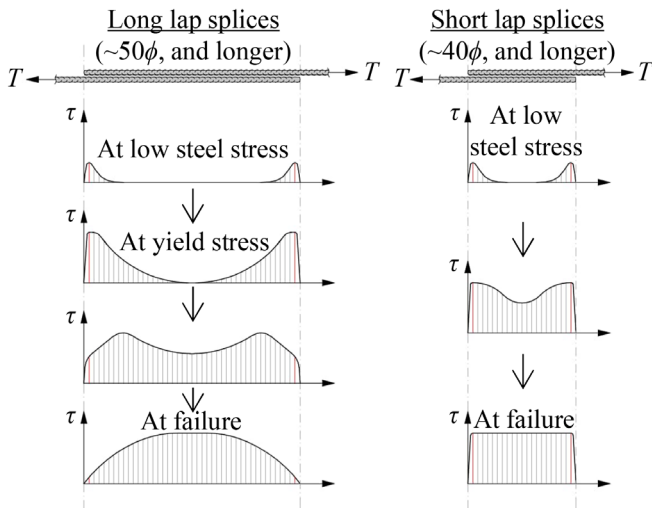


FIGURE 12 Typical bond-stress profiles in lap splices at different load levels

3.5 | Design recommendation for the laps close to plastic hinges

The test results of the 100% lapped test specimens are used to evaluate how much the lap length should be increased from required by yielding in order to reach the same total strains outside the lap splice before failure as in the corresponding beams without lap splices.

At first, a lap-spliced beam, whose ϵ_{sm} is as close as possible to the ϵ_{sm} value determined from the reference beam with the same bar size, is selected from each test

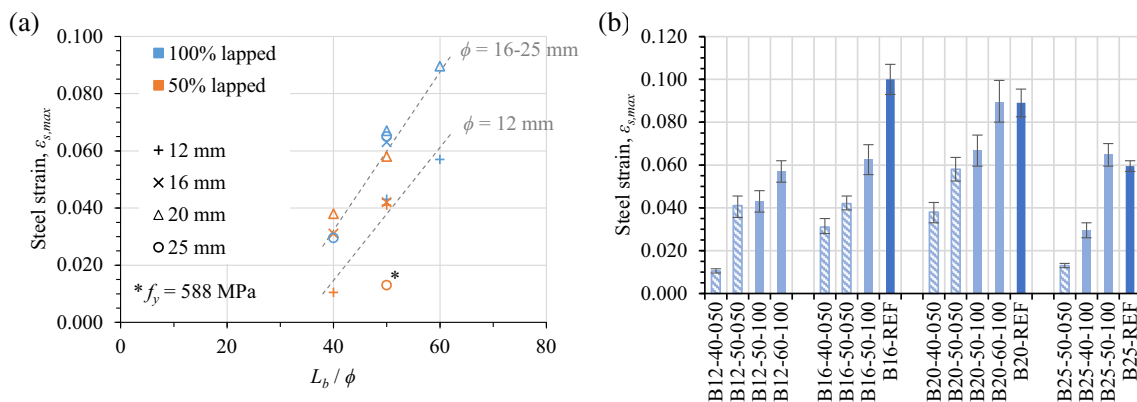


FIGURE 13 (a) Maximum steel strain at ultimate load of yielded test specimens with a lap splice calculated by using TCM. (b) Influence of crack spacing on determination of maximum steel strain.

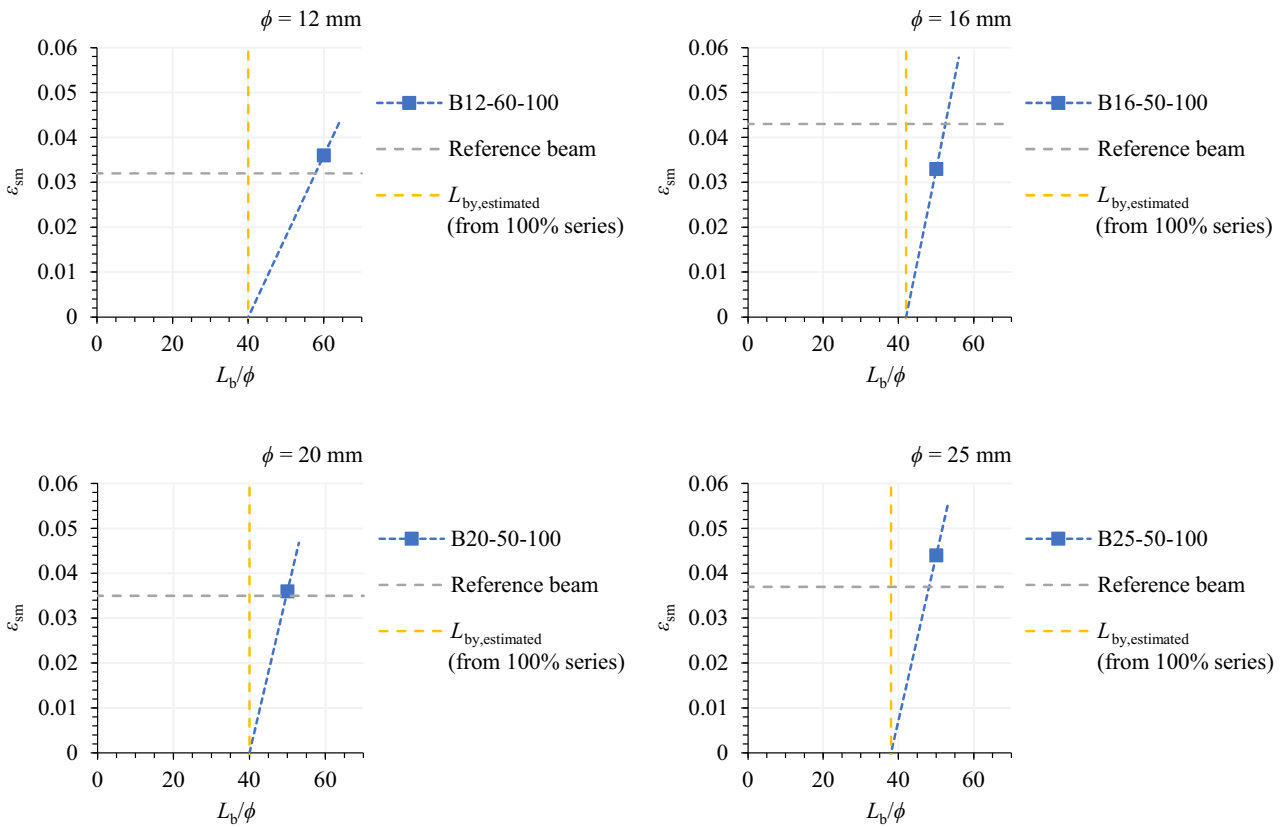


FIGURE 14 Determination of the lap length required to achieve equivalent total strains after the lap region as in beams without laps

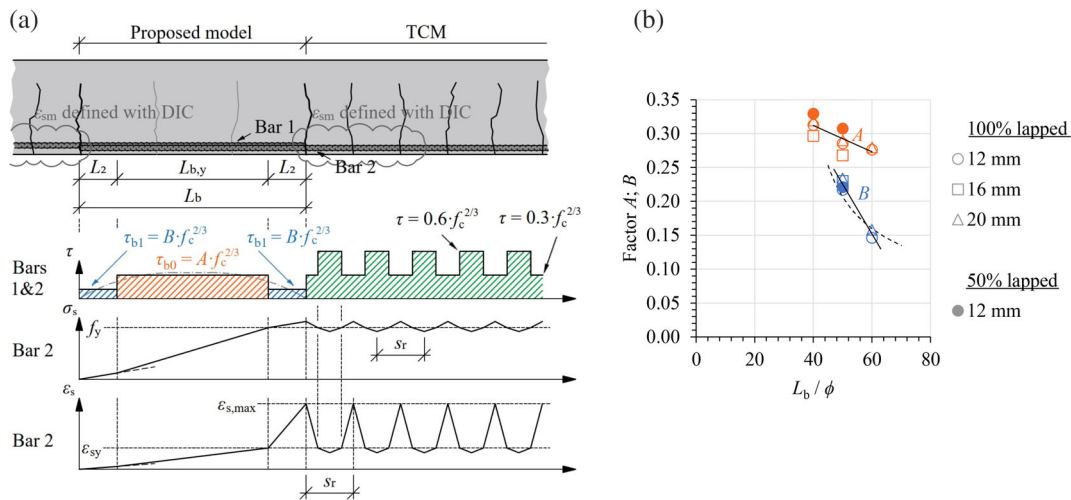


FIGURE 15 (a) Bond stress model for lap splice which reach the yielding in the spliced bars. (b) Bond stress factors for the selected test series.

series. Then, the lap length required by the yielding of the longitudinal bars is evaluated for all 100% lapped test series based on their moment-deflection relations. For evaluating the lap length required to reach the same total strains as in the reference beam, the linear interpolation is used as shown in Figure 14. Based on this analysis, the lap lengths should be 1.45, 1.25, 1.24, and 1.22 times the lap length required by the yielding for 12, 16, 20, and 25 mm bars, respectively. For medium- and large-diameter

bars ($\phi = 16, 20,$ and 25 mm), the results are close to each other, while for small-diameter bars ($\phi = 12$ mm) clearly longer lap length is needed. This is probably due to the fact that the 12 mm bars were straightened from the coil, and thus the stiffness of the reinforcement is still relatively high directly after yielding, as there is no yield plateau on their stress-strain curves.

It should be noted that this method includes several assumptions, and the number of the test specimens of

verifying this is small. However, based on the small variation of the results, it is shown that this gives results in the right order of magnitude. Based on the results, the lap length should be 1.2–1.3 times that length which is required by the yielding of the ordinary bars to achieve equivalent total strains after the lap region as in beams without laps. If the spliced bar is straightened from coil, that multiplying factor should be higher, around 1.5. It is also important to note, that the total rotation of the member with laps is still smaller because the strains are much smaller along the laps than on either side of the laps.

4 | ANALYTICAL MODEL

4.1 | Assumptions

The proposed model gives a tool to evaluate strains of bars on the lap. Outside the lap, the TCM is assumed (Figure 15). The difference between these areas is, that along the lap the stresses are transferred from one bar to another, whereas outside of the lap, the bar is anchored to the surrounding concrete between the cracks.

In the proposed analytical model for the bond-stress profiles in lap splices, after the yielding of the bars, the following assumptions are made, which are in many respects similar to the assumptions of TCM^{30,31}:

1. A stepped, rigid-perfectly plastic bond shear stress-slip relationship is used. The model assumes a constant bond stress, τ_{b0} , in the midsection of the lap splice for that length ($L_{b,y}$ in Figure 15a), which is required to transmit the yield stress of lapped bars, and a lower constant bond stress, τ_{b1} , for the other parts of the lap splice (L_2 in Figure 15a). Bond stress is assumed to be constant along the entire perimeter of the bar.
2. The lap length which is required to transmit the yield stress of lapped bars is experimentally known or evaluated using the lap strength model, e.g., the model presented in *fib* Bulletin 72.
3. The influence of the bending cracks is included in average bond stress value.
4. Bilinear and linear stress-strain relationships are assumed for the steel and for the concrete in tension, respectively.
5. Concrete does not have significant capability to withstand tensile strains.

4.2 | Bond behavior of lap splice in post-yield range

The bond stresses in the mid-section of the lap splice, τ_{b0} , and at the other parts of the lap splice, τ_{b1} , can be expressed in relation to the concrete tensile strength,

which is here presented as a function of the compressive strength:

$$\tau_{b0} = A \cdot f_c^{2/3}, \quad (4)$$

$$\tau_{b1} = B \cdot f_c^{2/3},$$

where A and B denote the coefficients which are assumed to be linearly proportional to L_2 . In the following paragraphs, these coefficients are calibrated against the test results.

In 100% lapped specimens with $\phi = 12$ –20 mm reinforcement and 50% lapped specimens with $\phi = 12$ mm reinforcement, the tested lap length of 40ϕ was found to be fairly accurately the length required to transfer the yield steel stress of bars on the basis of the deflection diagrams and the strain measurements. Since it is possible to evaluate the actual lap length required to transfer the yield steel stress of bars experimentally with sufficient accuracy, the results of these four series are compared to the proposed model.

The maximum steel stresses for the test beams of these examined test series are evaluated using a bilinear material model with strain hardening for the reinforcement, and steel strains determined via DIC technique, as shown in Equation 5. Test specimens with a lap length from 40ϕ to 60ϕ are used in this analysis. The constant bond stresses, τ_{b0} and τ_{b1} , at which the maximum reinforcement stress can be transferred according to Figure 15a are evaluated for the specimens (Figure 15b).

$$\sigma_{su} = f_y + (\varepsilon_{s,\max} - \varepsilon_{sy}) \cdot \frac{f_u - f_y}{\varepsilon_{su} - \varepsilon_{sy}}, \quad (5)$$

where f_y is the bar yield strength; f_u is the bar ultimate strength; $\varepsilon_{s,\max}$ is the maximum steel strain at the crack (determined via DIC technique using TCM); ε_{sy} is the yield strain of the bar; and ε_{su} is the ultimate strain of the bar.

4.3 | Comparison with experimental results

The results show a decrease of the apparent bond stress in these specimens when the lap length is increased. The experimental results in Figure 15b show that the relation between the apparent bond stresses and L_b/ϕ is approximately linear, this being an indication on the suitability of the proposed model in the case of long lap splices. However, the bond stress at the end of the lap may be

negligible, as shown in Figure 11. This can also be observed in Figure 15b, where the average bond stress from lap length 50ϕ to 60ϕ is remarkably reduced. Therefore, the maximum length of L_2 in the proposed model should probably be limited, which is logical when compared to the common bond-slip models with large slip values (*fib* Model Code 2010¹⁴). Based on this study, the authors suggest the value of 10 bar diameters as the upper limit for L_2 , because the bond stress between 50ϕ and 60ϕ lap lengths is already quite low. More test results, however, are needed to assess the effectiveness of the proposed model, with specific reference to lap splices longer than those examined in this paper.

5 | CONCLUSIONS

Thirty-four reinforced-concrete beams provided with lap splices at midspan and four reference beams without lap splices were tested in four-point bending, with the following results:

1. Any lap length exceeding the length required by the yielding of the reinforcing bars makes the lap splice more ductile. Consequently, in any lap splice placed in a region where a plastic hinge is expected to form, the lap length should be designed to be greater than that required by the yielding of the bars, to guarantee sufficient ductility. The authors propose the lap length to be multiplied around 1.2–1.3 from that required for yielding for the ordinary bar if the lap splice is close to the section where plastic strains are expected to localize in order to achieve equivalent total strains after the lap region as in beams without laps. If the spliced bar is straightened from coil, the multiplying factor should be higher, around 1.5.
2. In long lap splices, the formation of the plastic hinges occurs at the ends of the splice where the plastic deformations are the largest. At the same time, the deformations in the mid-region of the splice are definitely lower because of the total reinforcement, which might be even twice as much as that of the regions outside the splice.
3. The plastic deformations in the two cases in which 50% or 100% of the reinforcement is spliced do not exhibit any sizeable difference until post-peak behavior is reached. However, the role played by the distance between a given spliced bar and the nearest stirrup leg requires further studies.
4. The moment-deflection response in the RC beams reinforced with small-diameter bars obtained from coils ($\phi = 12$ mm) exhibits some differences with respect to the response of the beams reinforced with

- medium- and large-diameter bars ($\phi = 16, 20,$ and 25 mm), as in the former case a sharp yield point cannot be defined from the moment-deflection response, and the maximum steel strains at the crack interfaces are lower at beam's failure. A possible explanation comes (a) from the different stress–strain curves of the small-diameter bars, that were straightened from coils, and (b) from the highest relative rib area (f_R value) of the tested bars that influences to a lower crack spacing.
5. A realistic, sufficiently simple model is proposed for the bond-stress distribution along the lap splice after the yielding of the bars. A constant bond-stress profile is assumed for the mid-region of the splice, for a lap length equal to that required to transfer force in the bars at yielding, while in the remaining parts of the splice (at its extremes), the constant bond stresses are lower. Further studies are needed to refine the proposed model.

ACKNOWLEDGMENTS


The authors would like to acknowledge the financial support provided by the Finnish Concrete Industry. The authors are grateful to the laboratory personnel, particularly M.Sc. Tomi Strander and B.Sc. Lauri Kuusisto for their valuable contribution for this research.

DATA AVAILABILITY STATEMENT

The data that support the findings of this study are available from the corresponding author upon reasonable request.

ORCID

Jukka Haavisto  <https://orcid.org/0000-0003-0083-0701>

Anssi Laaksonen  <https://orcid.org/0000-0001-8459-7470>

REFERENCES

1. fib Bulletin No 72 Bond and anchorage of embedded reinforcement: background to the fib model code for concrete structures 2010. Lausanne: fib; 2014.
2. Orangun CO, Jirsa JO, Breen JE. A reevaluation of test data on development length and splices. *ACI J Proc.* 1977;74(3):114–22.
3. Canbay E, Frosch RJ. Bond strength of lap-spliced bars. *ACI Struct J.* 2005;102(4):605–14.
4. Esfahani MR, Kianoush MR. Development/splice length of reinforcing bars. *ACI Struct J.* 2005;102(1):22–30.
5. Cairns J. Bond and anchorage of embedded steel reinforcement in fib model code 2010. *Struct Concr.* 2015;16(1):45–55. <https://doi.org/10.1002/suco.201400043>
6. Schoening JC. Anchorages and laps in reinforced concrete members under monotonic loading. Germany: RWTH Aachen University; 2018.
7. Chinn J, Ferguson PM, Thompson JN. Lapped splices in reinforced concrete beams. *ACI J Proc.* 1955;52(10):201–13.

8. Ferguson PM, Breen JE. Lapped splices for high strength reinforcing bars. *ACI JProc.* 1965;62(9):1063–78. <https://doi.org/10.14359/7738>
9. Tepfers R. A theory of bond applied to overlapped tensile reinforcement splices for deformed bars. Gothenburg: Chalmers University of Technology; 1973.
10. Rezanoff T, Konkankar US, Fu YC. Confinement limits for tension lap splices under static loading. *Can J Civ Eng.* 1992; 19(3):447–53. <https://doi.org/10.1139/l92-054>
11. Azizinamini A, Darwin D, Eligehausen R, Pavel R, Ghosh SK. Proposed modifications to ACI 318-95 tension development and lap splice for high-strength concrete. *ACI Struct J.* 1999; 96(6):922–6.
12. Zuo J, Darwin D. Splice strength of conventional and high relative rib area bars in Normal and high-strength concrete. *ACI Struct J.* 2000;97(4):630–41. <https://doi.org/10.14359/7428>
13. *fib Task Group 4.5 “Bond models,” Splice test database.* (2005). http://fibtg45.dii.unile.it/files_scaricabili/0A0Database_splicetest Stuttgart sept 2005.xls
14. *fib Model Code 2010. Model Code for Concrete Structures 2010.* Berlin: Ernst & Sohn; 2013.
15. *CEB-FIP Model Code 1990. Model Code for Concrete Structures 1990.* London: Thomas Telford Ltd.; 1990.
16. prEN 1992-1-1:2020 D7 Eurocode 2: design of concrete structures -part 1–1: general rules, rules for buildings, bridges and civil engineering structures. Brussels: European Committee for Standardization; 2020.
17. EN 1992-1-1. Eurocode 2: Design of concrete structures - Part 1–1: General rules and rules for buildings. Brussels: European committee for standardization; 2015.
18. Darwin D, Zuo J, Tholen ML, Idun EK. Development length criteria for conventional and high relative rib area reinforcing bars. *ACI Struct J.* 1996;93(3):347–59.
19. Darwin D. Tension development length and lap splice design for reinforced concrete members. *Prog Struct Eng Mater.* 2005; 7(4):210–25. <https://doi.org/10.1002/pse.206>
20. Mousa MI. Flexural behaviour and ductility of high strength concrete (HSC) beams with tension lap splice. *Alex Eng J.* 2015;54(3):551–63. <https://doi.org/10.1016/j.aej.2015.03.032>
21. Azizinamini A, Pavel R, Hatfield E, Ghosh SK. Behavior of lap-spliced reinforcing bars embedded in high-strength concrete. *ACI Struct J.* 1999;96(5):826–35. <https://doi.org/10.14359/737>
22. Moodi Y, Sohrabi MR, Mousavi SR. Effects of stirrups in spliced region on the bond strength of corroded splices in reinforced concrete (RC) beams. *Constr Build Mater.* 2020;230: 116873. <https://doi.org/10.1016/j.conbuildmat.2019.116873>
23. Rakhshanimehr M, Esfahani MR, Kianoush MR, Mohammadzadeh BA, Mousavi SR. Flexural ductility of reinforced concrete beams with lap-spliced bars. *Can J Civ Eng.* 2014; 41(7):594–604. <https://doi.org/10.1139/cjce-2013-0074>
24. Mabrouk RTS, Mounir A. Behavior of RC beams with tension lap splices confined with transverse reinforcement using different types of concrete under pure bending. *Alex Eng J.* 2018;57: 1727–40. <https://doi.org/10.1016/j.aej.2017.05.001>
25. Gilbert RI, Kilpatrick AE. The strength and ductility of lapped splices of reinforcing bars in tension. *Aust J Struct Eng.* 2015; 16(1):35–46. <https://doi.org/10.7158/13287982.2015.11465177>
26. Gillani ASM, Lee S-G, Lee S-H, Lee H, Hong K-J. Local behavior of lap-spliced deformed rebars in reinforced concrete beams. *Materials.* 2021;14(23):7186. <https://doi.org/10.3390/ma14237186>
27. Turk K, Bassurucu M. An investigation on the effect of hybrid fiber reinforced on the flexural behavior of RC beams having different lap-spliced lengths. *Struct Concr.* 2022;1–13. <https://doi.org/10.1002/suco.202200106>
28. Micallef M, Vollum RL. The behaviour of long tension reinforcement laps. *Mag Concr Res.* 2018;70(14):739–55. <https://doi.org/10.1680/jmacr.17.00285>
29. Haefliger S, Kaufmann W, Thoma K. Modelling the load-deformation behaviour of lap splices with the tension chord model. *Eng Struct.* 2022;252:1–21. <https://doi.org/10.1016/j.engstruct.2021.113606>
30. Alvarez M. Einfluss des Verbundverhaltens auf das Verformungsvermögen von Stahlbeton. Switzerland: ETH Zürich; 1998.
31. Marti P, Alvarez M, Kaufmann W, Sigrist V. Tension chord model for structural concrete. *Struct Eng Int.* 1998;8(4):287–98. <https://doi.org/10.2749/101686698780488875>
32. EN 12350-2: 2019. Testing fresh concrete. Part 2: slump test. Brussels: European Committee for Standardization; 2019.
33. EN 12390-3: 2019. Testing hardened concrete. Part 3: compressive strength of test specimens. Brussels: European Committee for Standardization; 2019.
34. EN 12390-6: 2019. Testing hardened concrete. Part 6: tensile splitting strength of test specimens. Brussels: European Committee for Standardization; 2019.
35. EN ISO 15630-1: 2019. Steel for the reinforcement and prestressing of concrete. Test methods. Part 1: reinforcing bars, rods and wire. Brussels: European Committee for Standardization; 2019.
36. Cairns J, Jones K. Influence of rib geometry on strength of lapped joints: an experimental and analytical study. *Mag Concr Res.* 1995;47(172):253–62. <https://doi.org/10.1680/macrc.1995.47.172.253>
37. Metelli G, Plizzari GA. Influence of the relative rib area on bond behaviour. *Mag Concr Res.* 2014;66(6):277–94. <https://doi.org/10.1680/macrc.13.00198>
38. Moccia F, Ruiz MF, Metelli G, Muttoni A, Plizzari G. Casting position effects on bond performance of reinforcement bars. *Struct Concr.* 2021;22(3):1612–32. <https://doi.org/10.1002/suco.202000572>
39. Azizinamini A, Chisala M, Ghosh SK. Tension development length of reinforcing bars embedded in high-strength concrete. *Eng Struct.* 1995;17(7):512–22. [https://doi.org/10.1016/0141-0296\(95\)00096-P](https://doi.org/10.1016/0141-0296(95)00096-P)
40. Schoening J, Hegger J. Überprüfung der zusätzlichen Regeln für Ø40 mm nach EC2. *Beton- Und Stahlbetonbau.* 2015;110(9): 578–87. <https://doi.org/10.1002/best.201500031>
41. Haavisto, J., & Laaksonen, A. (2021). Test results and comparison to code equations on lap splice strength of reinforcement in RC beams. *Proc fib symposium 2021, Lisbon*, 887–896.
42. Maeda M, Otani S, Aoyama H. Effect of confinement on bond splitting behavior in reinforced concrete beams. *Struct Eng Int.* 1995;5(3):166–71. <https://doi.org/10.2749/101686695780601042>
43. Metelli G, Cairns J, Plizzari G. The influence of percentage of bars lapped on performance of splices. *Mater Struct.* 2015; 48(9):2983–96. <https://doi.org/10.1617/s11527-014-0371-y>
44. Metelli G, Marchina E, Plizzari GA. Effects of the position of confining transverse links on lap strength. *Struct Concr.* 2022; 23(5):2928–41. <https://doi.org/10.1002/suco.202100642>

45. ACI 318 building code requirements for structural concrete (ACI 318-19) and commentary (ACI 318R-19). Farmington Hills, Michigan: American Concrete Institute; 2019.
46. Cairns J. Staggered lap joints for tension reinforcement. *Struct Concr.* 2014;15(1):45-54. <https://doi.org/10.1002/suco.201300041>
47. Maurer, R., & Bettin, M. (2020). *Übergreifungslängen von Betonstahlbewehrung—Maßgebende Einflussparameter in den Grenzzuständen der Tragfähigkeit und Gebrauchstauglichkeit.* Heft B 148, BAST. Bremen: Fachverlag NW in der Carl Schöne-mann Verlag GmbH.



Anssi Laaksonen, Professor, Faculty of Built Environment—Concrete and Bridge Structures, Tampere University, Tampere, Finland. Email: anssi.laaksonen@tuni.fi.

AUTHOR BIOGRAPHIES



Jukka Haavisto, Researcher, Faculty of Built Environment—Concrete and Bridge Structures, Tampere University, Tampere, Finland. Email: jukka.haavisto@tuni.fi.



Heikki Alho, Researcher, Faculty of Built Environment—Concrete and Bridge Structures, Tampere University, Tampere, Finland. Email: heikki.alho@tuni.fi.

How to cite this article: Haavisto J, Alho H, Laaksonen A. Behavior of lap splices in reinforced concrete beams after bar yielding. *Structural Concrete.* 2023. <https://doi.org/10.1002/suco.202200501>